Chapter 1

Effects of Dielectric Substrate on Polarization Conversion Using Coupled Metasurfaces With and Without Tunneling

Andriy E. Serebryannikov, Mehmet Mutlu and Ekmel Ozbay

Additional information is available at the end of the chapter

http://dx.doi.org/10.5772/65950

Abstract

Dielectric substrates are technologically necessary components of various microwave and optical structures and devices, and may strongly affect their performance. For metasurfaces composed of subwavelength resonators, placing dielectric components in the proximity of resonators can lead to strong modification of subwavelength resonances and related transmission regimes. We focus on the effects exerted by material and geometrical parameters of such a dielectric substrate on linear-to-linear polarization conversion that appears in quasiplanar structures containing two coupled metasurfaces and enabling chirality. It is shown that spectral locations of the polarization conversion resonances and transmission efficiency at these resonances are strongly sensitive to the substrate parameters, whereas the ability of polarization conversion and related asymmetry of transmission can be preserved in wide ranges of parameter variation. The effects of a substrate are considered in detail for the mechanisms with and without tunneling, indicating a route to compact designs of quasiplanar structures for single- and multiband polarization conversion.

Keywords: metasurface, polarization conversion, subwavelength resonator, permittivity

1. Introduction

It is well known that material parameters of the components of an entire structure can strongly affect dispersion, transmission, and scattering characteristics. For some classes of the structures, such as the idealized lossless cavities and waveguides, effects of variation of the material parameters can be easily quantified. In particular, the rule of $\varepsilon^{-1/2}$, being applicable to eigenfrequencies of the closed cavities filled with a linear isotropic dielectric, is commonly known. The quantifying of resonances becomes much more complicated in the case of

open resonance structures, where the resonance fields can be strong beyond the resonators [1]. In this case, an a priori estimate of the strength of the effect of dielectric is very complicated and, moreover, one cannot predict the principal possibility of obtaining of a desired transmission regime. It can be even more difficult to preserve the same strength of some effects, e.g., efficiency of conversion of the incident wave energy to a certain diffraction order or polarization state, simultaneously with the shift of resonance frequencies, while only varying characteristics of the dielectric layer(s) adjacent to the resonators. Nevertheless, stacking resonant or nonresonant arrays with dielectric layers and placing dielectric components inside individual resonators are known as effective tools to control resonance frequencies and transmission and scattering characteristics [2–5].

Theory and technology related to subwavelength resonators have extensively been developed since the early 2000s. Initially, the interest to them has been stimulated by the possibility of obtaining artificial magnetism and negative refraction [6]. Later, a chiral way to negative refraction has been proposed, which is realized with the aid of planar metamaterials [7]. Artificial bianisotropic [8] and, in particular, electrically thin chiral structures based on metasurfaces composed of subwavelength resonators [9] have extensively been studied. The latter suggest efficient solutions for polarization conversion problem. Circular dichroism and polarization rotation belong to the most distinguished properties of the artificial chiral materials. One of the basic features is that electric and magnetic dipoles are strongly coupled and excited simultaneously, so that chirality originates from the collinear excitation of the effective electric and magnetic responses. Moreover, these responses can be switched at a fixed frequency by changing polarization of the incident electromagnetic wave. It is noteworthy that manipulation by polarization states can be achieved, in addition to the chiral structures, which are based on two coupled metasurfaces, with the aid of various other schemes and classes of the structures. In particular, high-contrast gratings, advanced quarter-wave plates, and structures with a single or multiple (anisotropic) metasurfaces can be mentioned [10–15].

In the coupled arrays of subwavelength resonators, conversion of the incident linear polarization to the circular polarization [16–21] and to the orthogonal linear polarization [22, 23] has been demonstrated. These conversions are directly related to *asymmetric transmission*, a Lorentz reciprocal phenomenon that enables strong forward-to-backward transmission contrast between two opposite incidence directions [22, 24–28]. Since reciprocity forbids one-way transmission in two-port reciprocal systems, asymmetric transmission requires breaking of spatial inversion symmetry and, hence, new transmission and reflection channels. For the twisted metasurfaces, they can be obtained by involving polarization states different from the incident one [16–18, 22, 29]. Diodelike asymmetric transmission with reflections vanishing for one of two opposite incidence directions has been theoretically predicted in the zero-loss approximation for both diffraction [30] and polarization conversion [1, 23] inspired mechanisms. The principal possibility of the perfect polarization conversion in a generalized double-layer structure has been demonstrated [31].

In one of the recent studies, linear-to-linear polarization conversion and diodelike asymmetric transmission in a thin chiral structure with 4-U unit cells have been obtained [23]. It was shown that the problem of their *perfectness* is an eigenstate, phase propagation, and impedance matching. It can be reached due to the coexistence of tunneling, optimization of the axial ratio

http://dx.doi.org/10.5772/65950

of the eigenwaves, and optimization of transmission phases of the eigenwaves that destructively interfere in one direction and constructively interfere in the opposite one. Recently, similar mechanisms have been realized in the structures with U-type unit cells, with and without an evanescent-wave metallic mesh and, thus, with and without tunneling [1]. Moreover, perfect multiband linear-to-linear polarization conversion and asymmetric transmission can be obtained with the aid of the coupled arrays of U-shaped apertures [32]. Besides, many recent studies should be mentioned which are dedicated to dual-band and broadband conversions of polarization that involve linear and circular states [1, 20, 21, 33–36].

In this chapter, the emphasis is put on the effects exerted by variations of the dielectric substrate parameters on subwavelength resonances and related regimes of linear-to-linear polarization conversion and asymmetric transmission. Consideration is restricted to quasiplanar structures containing two coupled metasurfaces that represent arrays of subwavelength split-ring resonators (SRRs) enabling simple U-type unit cells with resonant behavior at microwave frequencies, and to the case of normal incidence. Zero-loss approximation is utilized to clarify the main components of the underlying physical mechanisms. Two mechanisms will be discussed, which are realized in the structures with and without a metallic mesh (small-hole array) placed between the SRR arrays, i.e., tunneling either appears and contributes or does not. The focus will be on sensitivity of the subwavelength resonances in the studied structures with chirality to the variations in permittivity and thickness of the dielectric substrate layers located between the SRR arrays and the metallic mesh, or simply between two SRR arrays. Indeed, in the both cases, the resonance characteristics of individual resonators and those of the coupled metasurfaces can be strongly affected, because the resonators are placed directly on the dielectric layer(s). Perfect transmission that originates from the perfect matching of real impedances can be obtained in the mesh-free structures in some ranges of parameter variation. These ranges either coincide or do not coincide with the ranges, in which matching can appear for the structures with a mesh as a result of fulfillment of certain phase conditions. The role of the choice of permittivity and thickness of the dielectric layers can be very important for preserving the features related to the matching and perfect polarization conversion. While variations of substrate characteristics give big freedom in design without changes in SRR arrays, it can be further extended by a proper selection of an array period. Simulation results are obtained by using CST Microwave Studio, a full-wave commercial solver based on the finite integration method (see www.cst.com for software details). The same methodology can be applied to study the effects of a substrate for linear-to-circular and circular-to-circular polarization conversion in various structures based on metasurfaces. This chapter presents a review of the basic effects achievable by variations of substrate parameters in the structures with U-type assembly, while a comparative study of the existing and suggested performances for multi-/broadband polarization conversion is beyond its scope.

2. Polarization conversion, asymmetry in transmission and tunneling

First, let us briefly describe the structures to be studied that may enable polarization conversion and related asymmetry in transmission. Schematic of a unit cell and perspective view of the studied periodic structure are presented in **Figure 1**. Each of two SRR arrays has period of a

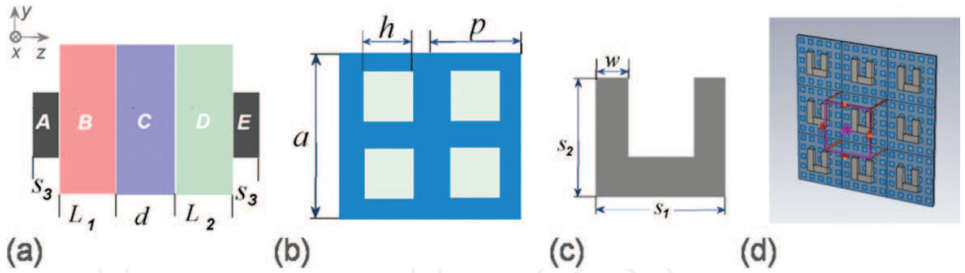

Figure 1. (a) Schematic of a complex unit cell (side view): A—SRR, B and D—dielectric layers with permittivity ε_1 and ε_2, respectively, C—metallic mesh, E—rotated SRR. (b) Metallic mesh with square holes seen from the frontside and backside at $a = 2p$. (c) SRR seen from the backside (denoted by E in the side view). (d) $(3a) \times (3a)$ fragment of the basic configuration at $a = 5p$ (perspective view).

in the x and y directions. The metallic mesh with thickness d and period p is obtained by periodic arrangement of the square holes, i.e., $a > p$; p is assumed to be the same over x and y. For the *basic configuration* with the metallic mesh [1], we take a = 22 mm, p = 4.4 mm, h = 2.2 mm, $L_1 = L_2$ = 1.25 mm, d = 0.5 mm, $s_1 = s_2$ = 10 mm, s_3 = 1.5 mm, and w = 3 mm. Hence, the total thickness of the structure is $S = d + 2s_3 + L_1 + L_2$. The back-side SRR array represents the front-side SRR array rotated by 90° in the clockwise direction. Such a location of the SRR arrays can create chirality and, thus, the ability of polarization conversion. The stronger the conversion, the stronger asymmetry in the transmission. In fact, the ability of asymmetric transmission originates from the fact that conversion of the incident wave is distinguished at front-side illumination and at back-side illumination, so that the different channels (e.g., that associated with the orthogonal polarization in transmission mode for the former, and that associated with the same polarization in reflection mode for the latter) are the main acceptors of the incident wave energy.

The use of the layers with $\varepsilon < 0$ (metallic mesh) and $\varepsilon > 0$ (dielectric substrate) in the same structure should allow one obtaining destructive interferences of the waves reflected at the interfaces between the layers from A to E and those between air and the layers A and E. This can result in zero reflection and, accordingly, in perfect tunneling. Generally, the operation is based on wave interference, and, thus, the phase is a critical parameter. However, a negative-ε layer is not necessary for obtaining of zero reflections, if input impedances at the interfaces of the individual layers are properly adjusted. This is a reason why similar regimes of polarization conversion can be obtained in the structures with and without a metallic mesh and, thus, the mechanisms with and without tunneling are worth comparing [1].

In the general case, a linearly polarized incident wave changes its polarization state when passing through such a coupled system. The complex amplitudes of the incident ($E_{xi}^{f,b}$ and $E_{yi}^{f,b}$) and transmitted ($E_x^{f,b}$ and $E_y^{f,b}$) waves are expressed through each other with the aid of the T-matrix as follows [22, 23]:

$$\begin{pmatrix} E_x^{f,b} \\ E_y^{f,b} \end{pmatrix} = \begin{pmatrix} T_{xx}^{f,b} & T_{xy}^{f,b} \\ T_{yx}^{f,b} & T_{yy}^{f,b} \end{pmatrix} \begin{pmatrix} E_{xi}^{f,b} \\ E_{yi}^{f,b} \end{pmatrix}, \tag{1}$$

where $E_{xi}^{f,b}$ and $E_{yi}^{f,b}$ are the x and y components of the incident wave; $T_{xx}^{f,b}$ and $T_{yy}^{f,b}$ are the *copolarized* transmission coefficients, and $T_{xy}^{f,b}$ and $T_{yx}^{f,b}$ are the *cross-polarized* transmission

coefficients, f and b stand for the forward and the backward transmission cases, which correspond to front-side and back-side illumination, respectively.

The amplitudes in these two cases are related to each other, depending on the structural symmetries. For the structures showing the same symmetries as the studied one, $T^f_{xy} = -T^b_{yx}$, $T^f_{yx} = -T^b_{xy}$ and $T^f_{xx} = T^b_{xx} = T^f_{yy} = T^b_{yy}$, provided that $\varepsilon = \varepsilon_1 = \varepsilon_2$. According to references [23, 29], if the structure parameters can be adjusted so that $T^{f,b}_{xx} = 0$, $T^{f,b}_{yy} = 0$, $T^f_{yx} = T^b_{xy} = 0$ and $|T^f_{xy}| = |T^b_{yx}| = 1$ at some resonances, then perfect linear-to-linear polarization conversion is achieved. This regime is schematically illustrated in **Figure 2(a)**, where transmission, reflection, and polarization conversion are explained by using a four-port system. Perfect polarization conversion and perfect asymmetry in transmission may occur when either y-polarized plane wave is incident from the frontside, or x-polarized plane wave is incident from the backside. In turn, if either y-polarized wave is incident from the backside, or x-polarized wave is incident from the frontside, perfect reflection takes place. As a result, transmission may be strong at either front-side or back-side illumination, depending on which of two incident linear polarizations is utilized. At the same time, it vanishes at the opposite-side illumination when the same polarization state of the incident wave is used. Clearly, this reversibility of the direction of diodelike transmission occurs when the incident polarization is changed (for the both incidence directions) to the orthogonal one, because Lorentz reciprocity forces the scattering matrix to be symmetric.

It may occur that at the other polarization conversion resonances the above-described operation regime appears when $T^{f,b}_{xx} = 0$, $T^{f,b}_{yy} = 0$, $T^b_{yx} = T^f_{xy} = 0$ and $|T^b_{xy}| = |T^f_{yx}| = 1$. In this case, the schematic in **Figure 2(a)** should be modified, i.e., the ports with perfect reflection and those with perfect transmission replace each other.

For the circularly polarized (CP) waves, we have, instead of Eq. (1),

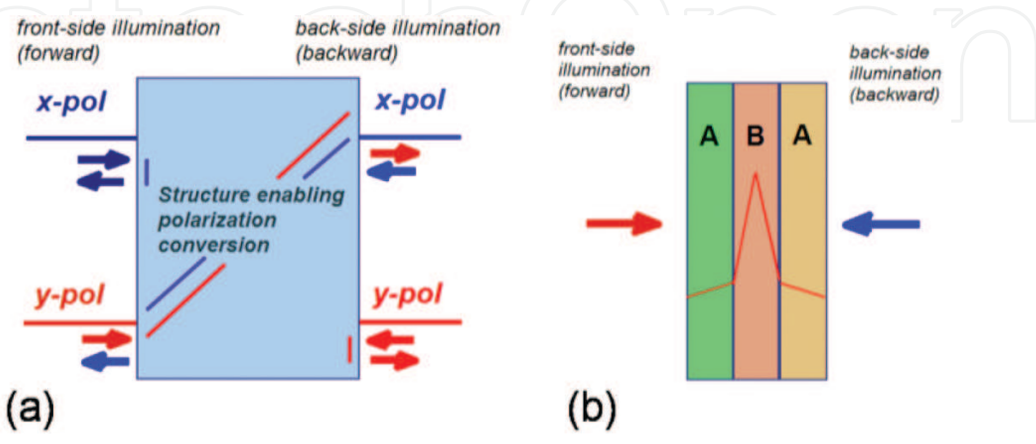

Figure 2. (a) Schematic of perfect polarization conversion and asymmetric transmission regime. (b) Schematic of tunneling in ABA-type stack with propagating-wave layers A and evanescent-wave layer B; red line shows possible (simplified) variation of the field magnitude in the propagation (normal) direction.

$$\begin{pmatrix} E_{+}^{f,b} \\ E_{-}^{f,b} \end{pmatrix} = \begin{pmatrix} T_{++}^{f,b} & T_{+-}^{f,b} \\ T_{-+}^{f,b} & T_{--}^{f,b} \end{pmatrix} \begin{pmatrix} E_{+i}^{f,b} \\ E_{-i}^{f,b} \end{pmatrix}, \tag{2}$$

where $E_{+i}^{f,b}$ and $E_{-i}^{f,b}$ are the components of the incident wave that correspond to right- and left-handed CP waves; $T_{++}^{f,b}$ and $T_{--}^{f,b}$ are the transmission coefficients of right- and left-handed CP waves, and $T_{+-}^{f,b}$ and $T_{-+}^{f,b}$ are the cross-coupling transmission coefficients, superscripts f and b indicate the forward and backward transmission cases; $T_{++}^{f,b} = T_{xx}^{f,b} + T_{yy}^{f,b} + i(T_{xy}^{f,b} - T_{yx}^{f,b})$, $T_{--}^{f,b} = T_{xx}^{f,b} + T_{yy}^{f,b} - i(T_{xy}^{f,b} - T_{yx}^{f,b})$, $T_{+-}^{f,b} = T_{xx}^{f,b} - T_{yy}^{f,b} - i(T_{xy}^{f,b} + T_{yx}^{f,b})$, $T_{-+}^{f,b} = T_{xx}^{f,b} - T_{yy}^{f,b} + i(T_{xy}^{f,b} + T_{yx}^{f,b})$, $T_{-+}^{f} = T_{+-}^{b}$ and $T_{+-}^{f} = T_{-+}^{b}$. Efficient polarization conversion and asymmetry in transmission can also be obtained for the CP waves [18, 19, 21, 36]. However, the focus in this chapter is related to the effects arising for the linearly polarized waves.

For a part of the structures considered here, tunneling is an important component of the resulting polarization conversion mechanism that has initially been suggested in reference [23]. Previously, a similar tunneling-based mechanism has been utilized for obtaining perfect transmission through the sandwiched structures comprising evanescent-wave layers, which do not enable polarization conversion [37–39]. In particular, it was shown that arrays of subwavelength resonators may play two roles: either work as positive-ε layers in the tunneling mechanism or contribute to the effective negative-index behavior.

The general idea of matching in case of the presence of evanescent-wave components can be explained in terms of transmission through isotropic AB type (bilayer) and ABA type (trilayer) stacks, in which A and B stand for propagating-wave and evanescent-wave layers, respectively, see **Figure 2(b)**. According to reference [37], the criterion of the perfect transmission for AB stack can be written as follows:

$$(k_1/k_0 - k_0/k_1)tan(k_1d_1) - (\alpha_2/k_0 + k_0/\alpha_2)tanh(\alpha_2d_2) + i(k_1/\alpha_2 + \alpha_2/k_1)tan(k_1d_1)tanh(\alpha_2d_2) = 0, \tag{3}$$

where k_1 and d_1 are wave number and thickness of the layer A, $k_2 = i\alpha_2$ and d_2 are wave number and thickness of the layer B. This criterion cannot be satisfied, since the second term is imaginary, i.e., the waves scattered by the layers A and B, being in different phase planes, cannot entirely cancel each other. Then, if we add one more layer A, as shown in **Figure 2(b)**, the criterion can be rewritten as follows:

$$\begin{aligned}(k_1/k_0 - k_0/k_1)2tan(k_1d_1) - (\alpha_2/k_0 + k_0/\alpha_2)tanh(\alpha_2d_2) - [k_1^2/(\alpha_2k_0) \\ + (\alpha_2k_0)/k_1^2]tan^2(k_1d_1)tanh(\alpha_2d_2) = 0.\end{aligned} \tag{4}$$

Now, both the first and the second term are real and, thus, Eq. (4) has a solution that corresponds to the perfect transmission. This model enables a qualitative but physically correct prediction of the perfect transmission also for complex anisotropic structures with the polarization conversion ability, including the case of coupled metasurfaces with a metallic mesh [23]. For the structures without a mesh and, hence, without tunneling, conditions of the perfect

transmission can easily be obtained from matching of impedances. For an ABA-type stack, this yields

$$tan(k_1 d_1) = 0 \text{ and } tan(k_2 d_2) = 0, \tag{5}$$

where k_2 is real wave number of the layer B. In the next sections, the existence, efficiency, and generality of polarization conversion achievable in ABA-type stacks at variations of substrate parameters will be discussed.

3. Varying characteristics of dielectric substrate

3.1. Basic effects of substrate permittivity

Here, we demonstrate how the choice of a dielectric substrate material can affect the ability and manifestations of polarization conversion in the structures based on coupled metasurfaces. Let us consider the case of an intermediate distance between metasurfaces and vary ε from 1 (substrate-free case) to 40 (some types of ceramics, e.g., see reference [40]). In **Figure 3**, results are presented for the structures with and without a mesh. In the latter case, it is assumed that the mesh is simply removed from the mesh-containing structures, and a homogeneous dielectric layer fully occupies the region between two metasurfaces. Then, its thickness is $L = d + L_1 + L_2$. To better illustrate the basic features, we first consider the case of ε = 1, see **Figure 3(b, c)**. For the mesh-free structure in **Figure 3(b)**, polarization conversion is observed between 6 and 8 GHz. However, all of the diagonal and nondiagonal components of the *T*-matrix are of the same order, so that a nearly perfect one-way linear-to-linear polarization conversion and relevant diodelike transmission cannot be obtained. At the same time, conversion into polarization states being different from a linear one can be quite strong. The twin maxima like those shown in **Figure 3(b)** are typical for the coupled SRR arrays. They may appear regardless of whether polarization conversion is possible or not, and can be explained by using Lagrange (hybridization) formalism [9, 41–43]. The strength of coupling can be utilized to control optical activity and polarization conversion. In particular, either two narrow bands of polarization conversion, which are well separated from each other, or a wide band with two weak maxima might be obtained.

Each SRR can approximately be presented as an LC circuit, with inductance L and capacitance C, and resonance angular frequency $\omega_0 = (LC)^{-1/2}$. Accordingly, the Lagrangian of a single SRR can be written as $\Gamma = (L/2)(\dot{q}^2 - \omega_0^2 q^2)$, where q stands for a charge that is considered as a generalized coordinate. In the case of two coupled SRRs that belong to different metasurfaces, the Lagrangian represents the sum of the Lagrangians of two individual SRRs plus the coupling term, i.e.

$$\Gamma = (L/2)(\dot{q}_1^2 - \omega_0^2 q_1^2) + (L/2)(\dot{q}_2^2 - \omega_0^2 q_2^2) + M\dot{q}_1\dot{q}_2, \tag{6}$$

where q_1 and q_2 correspond to the first and the second SRR, respectively, and M is mutual inductance arising due to the magnetic coupling of two SRRs. Magnetic coupling is considered

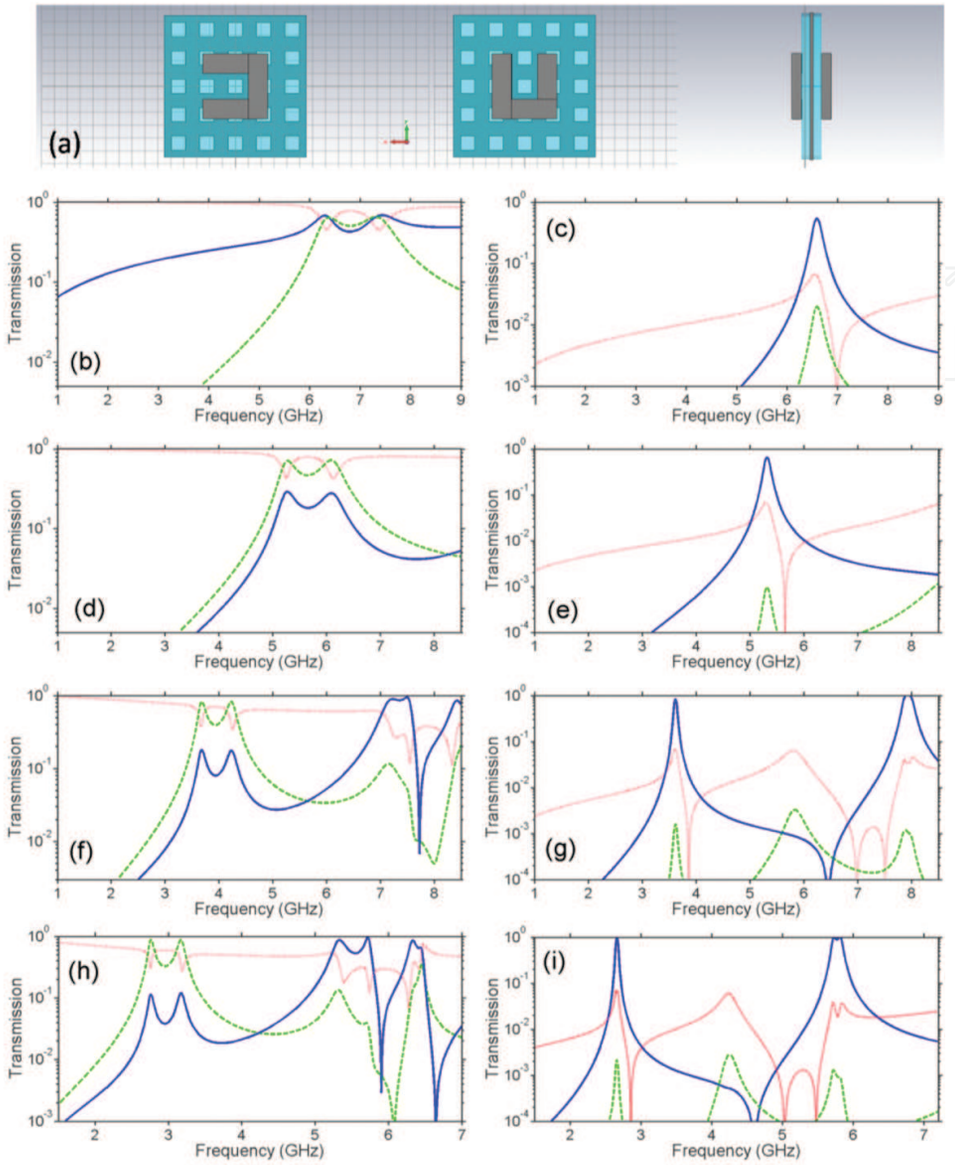

Figure 3. (a) Front, back, and side view of a unit cell, and transmission for the basic configuration (b, d, f, h) without and (c, e, g, i) with metallic mesh; (b, c) $\varepsilon = 1$, (d, e) $\varepsilon = 2.1$, (f, g) $\varepsilon = 5.8$, (h, i) $\varepsilon = 11.4$; solid blue line – $|T^f_{xy}| = |T^b_{yx}|$, dashed green line – $|T^f_{yx}| = |T^b_{xy}|$, and dotted red line – $|T^f_{xx}| = |T^b_{xx}| = |T^f_{yy}| = |T^b_{yy}|$.

to be independent of the angle of rotation of the second SRR [43]. The eigenfrequencies are given by $\omega_{\pm} = \omega_0[1 \mp (M/L)]^{-1/2}$, where ω_+ and ω_- correspond to an antisymmetric and a symmetric charge distribution, respectively [41]. Hence, a spectral distance between the eigenfrequencies is

$$\Delta\omega = \omega_+ - \omega_- \approx (M/L)\omega_0. \tag{7}$$

Mutual inductance quickly decreases while the distance between SRRs is increased and, thus, the spectral separation becomes smaller. Electric coupling of two SRRs, which depends on the rotation angle, can be easily involved into this model [9, 43].

For the structure with the metallic mesh in **Figure 3(c)**, the diagonal components and one of the nondiagonal components of the *T*-matrix are suppressed, as desired. As a result, one-way polarization conversion can be obtained. However, a nearly perfect transmission is again not reached: $max|T^f_{xy}| = 0.54$ and $max|T^b_{yy}| = 0.067$ at $f = 6.59$ GHz. On the contrary to the mesh-containing structure with 4U-type unit cells [23] and the mesh-free structure in **Figure 3(b)**, the unwanted components of the *T*-matrix are well suppressed, enabling strong directional selectivity in a wide frequency band. Note that the mesh alone only allows one obtaining a very weak transmission in this band, i.e., evanescent-wave regime is evident. In this case, Lagrange formalism in the above-presented form is not applicable, since additional modifications are required to properly take into account the effects of the mesh.

Placing a low-ε layer between two metasurfaces in the mesh-free configurations and between each metasurface and the mesh in the mesh-containing configurations results in that all of the basic transmission and polarization conversion features observed in **Figure 3(b, c)** are preserved, while the resonance frequencies are redshifted. This is quite expectable, although the obtained shift is weaker than it would be when the rule of $\varepsilon^{-1/2}$ is valid. In **Figure 3(d, e)**, we use a material with $\varepsilon = 2.1$ that belongs to the ε-range, to which many materials that are widely used at microwave and optical frequencies (e.g., polytetrafluoroethylene/Teflon, SiO_2) do belong. In particular, the first maximum of $|T^f_{xy}|$ in the case of the mesh-containing structure is redshifted from $f = 6.59$ to $f = 5.29$ GHz, compare **Figure 3(c, e)**. In turn, two first maxima of $|T^f_{yx}|$ in the case of the mesh-free structures are redshifted from $f = 6.35$ and $f = 7.3$ GHz to $f = 5.27$ and $f = 6.09$ GHz, respectively, see **Figure 3(b, d)** for comparison. Moreover, the maximal values of $|T^f_{yx}|$ shown in **Figure 3(d)** are several times larger than the values of $|T^f_{xy}|$ at the same frequencies. The maximal values of $|T^f_{xy}|$ in **Figure 3(d, e)** become closer to unity, so the nearly perfect conversion regime is approached.

The above-discussed features can be enhanced at a further increase of ε. In **Figure 3(f, g)**, the results are presented for $\varepsilon = 5.8$ (e.g., some types of glass and diamond). Now, we obtain $max|T^f_{yx}| > 0.8$ at $f = 3.67$ and $f = 4.22$ GHz, and $max|T^f_{xy}| > 0.89$ at $f = 7.22$ and $f = 7.49$ GHz for the mesh-free structure in **Figure 3(f)**, and $max|T^f_{xy}| > 0.8$ at $f = 3.6$ GHz, and $max|T^f_{xy}| > 0.995$ near $f = 7.9$ GHz for the mesh-containing structure in **Figure 3(g)**, while the second cross-polarized component is well suppressed. Higher resonances are redshifted so that dual-band operation with a large distance between the bands is possible at $f < 8.5$ GHz. Note that $S/\lambda < 0.17$ and $a/\lambda < 0.62$ at $f < 8.5$ GHz, where λ is the free-space wavelength.

What can be even more important for practical applications is that the high-frequency polarization conversion band at $f > 7$ GHz is wider than those connected with the maxima near $f = 4$ GHz, in **Figure 3(f, g)**. If single-band operation is sufficient, design can be optimized based on the trade-off between the bandwidth and electrical size. It is worth noting that a part of the near-unity transmission scenarios is realized by using the *y*-polarized incident wave, while the other part does with the aid of the *x*-polarized incident wave. In particular, for the mesh-free structure in **Figure 3(f)** we obtain different directions of near-unity transmission for the first two maxima and for the high-frequency band, while this direction is the same for the both bands in the mesh-containing structure in **Figure 3(g)**.

While the maxima twinning is a general feature shown by the mesh-free structures, there is no twinning for the mesh-containing structures. The absence of twinning may originate from the merging of the maxima, which correspond to different but very weakly separated resonances. An additional study based on Lagrange formalism or other models of resonance coupling is required to clarify this difference. Due to the Lorentz reciprocity, a nearly perfect polarization conversion is a one-way effect. Indeed, if the same polarization state is used at both frontside and backside illumination, we obtain the perfect reflection for illumination from the side being opposite to that one, at which a nearly perfect polarization conversion is obtained. A key feature is that the copolarized components are well suppressed in a wide frequency range, including the polarization conversion bands. Up to now, the mesh free and the mesh-containing performances that contain the dielectric layers with ε = 5.8 have been the best among the discussed ones in terms of conversion efficiency, suppression of the unwanted components, and number of the achievable conversion bands.

Next, we investigate whether we have more flexibility in choice of ε, i.e., whether the basic features observed in **Figure 3(f, g)** can be kept when a higher-ε material (i.e., with $\varepsilon > 5.8$) is used for the dielectric layers. Indeed, since the resonance frequencies are expected to be further redshifted, the desired values of impedances, phases, and efficiency of one-way polarization conversion are not guaranteed. **Figure 3(h, i)** present the transmission results for the two structures at $\varepsilon = 11.4$. The chosen value of ε corresponds to the range, to which many materials such as graphite, Si, and GaAs are belonging. By comparing to **Figure 3(f, g)**, the spectra shown in **Figure 3(h, i)** are very similar but are much denser. For instance, the dependences in **Figure 3 (f)** at $f < 8.5$ GHz are similar to those in **Figure 3(h)** at $f < 6.3$ GHz, so that changing a scale at the abscissa axis would make these dependences almost identical. The same remains true for the dependences in **Figure 3(g)** at $f < 8.5$ GHz and those in **Figure 3(i)** at $f < 6.3$ GHz. In **Figure 3(h)**, we obtain $max|T^f_{yx}| = 0.885$ and $max|T^f_{yx}| = 0.88$ at f = 2.76 and f = 3.14 GHz, respectively, whereas $|T^f_{xy}| = 0.87$ and $|T^f_{xy}| = 0.96$ for two maxima in the vicinity of f = 5.5 GHz. Thus, the cross-polarized components with magnitudes higher than 0.9 can be obtained even without a metallic mesh and tunneling, i.e., only due to matching of the real input impedances. In spite of that the copolarized components are still significant, high-efficiency transmission and polarization conversion are possible for this structure at two different incident polarizations.

From the *broadband* operation perspective, bringing the neighboring resonances together might be useful, as shown in **Figure 3(i)** around 5.76 GHz for the structure with the mesh. Indeed, such a coupling of two resonances can be obtained that the dip between the neighboring maxima is very weak and two neighboring bands are merged. In this regime, $|T^f_{xy}| > 0.99$ at the maxima, whereas $min|T^f_{xy}| = 0.88$ between them. Thus, the vicinity of f = 5.76 GHz can be suggested for broadband operation. One more high-efficiency polarization conversion band occurs at f = 2.66 GHz, where $max|T^f_{xy}| \approx 0.94$. Note that $a/\lambda \approx 0.2$ and $S/\lambda \approx 0.05$, and $a/\lambda \approx 0.42$ and $S/\lambda \approx 0.12$ at f = 2.66 GHz and f = 5.76 GHz, respectively.

Based on the obtained results, one can conclude that the main functions of the high-ε layers include redshift of the resonances, at which polarization conversion may occur, and improvement

of the phase and/or real impedance matching, which results in that the regime of perfect one-way polarization conversion is approached. The functions of the mesh include suppression of the unwanted components of the *T*-matrix and the collaborative effect with the high-ε layers and SRR arrays in the tunneling mechanism. In turn, the coupled SRR arrays enable polarization conversion, on the one hand, and contribute to the resulting transmission mechanism due to either tunneling or real impedance matching, on the other hand. The role of the SRR arrays here is similar, in principle, to that in the structures with 4U-type unit cells [23]. However, wideband suppression of the unwanted components has not been reached therein, in contrast with the results shown in **Figure 3**. To compare, transmission for the structures obtained from those in **Figure 3(c, e, g, i)** by removing the SRR arrays remains low, i.e., $|T^f_{xx}| = |T^f_{yy}| < 0.1$ and $|T^f_{xy}| = |T^b_{yx}| = 0$. Hence, the roles of the different structural components in obtaining of the nearly perfect matching and tunneling are clear.

The above-discussed features are kept even in wider ranges of variation of the problem parameters, including very high values of ε. For example, for the mesh-free structure similar to those in **Figure 3** but with ε = 35.4, we obtain the maxima of $|T^f_{yx}| = 0.96$ and $|T^f_{yx}| = 0.94$ at f = 1.63 and f = 1.87 GHz, respectively. The values of $|T^f_{xy}|$ that are equal to 0.86, 0.97, 0.88, 0.86, 0.92, and 0.98 correspond to the well-separated peaks located at 3.11, 3.4, 3.72, 4.32, 4.49, and 4.69 GHz, respectively. Among them, there are four narrow bands, in which either $|T^f_{xy}| > 0.99$ ($|T^b_{xy}| \approx 0$) or $|T^f_{yx}| > 0.99$ ($|T^b_{yx}| \approx 0$). More than five bands of high-efficiency, one-way polarization conversion can be easily obtained in one structure at subwavelength scale, i.e., at $a/\lambda < 0.5$ and $S/\lambda < 0.5$. This structure is really very thin as compared to λ, e.g., $S/\lambda \approx 0.03$ at f = 1.63 GHz and $S/\lambda \approx 0.09$ at f = 4.69 GHz. Note that $\varepsilon^{1/2}L/\lambda \approx 0.095$ and $\varepsilon^{1/2}L/\lambda \approx 0.28$, respectively. Thus, classical Fabry-Perot resonances in the dielectric layer are not expected to contribute to the resulting transmission mechanism that distinguishes our structures from those studied by Markovich et al. [31]. For the mesh-containing structure with ε = 35.4, we obtain four maxima, at which either $|T^f_{xy}| > 0.99$ ($T^b_{xy} \approx 0$), or $|T^f_{yx}| > 0.99$ ($T^b_{yx} \approx 0$), whereas $S/\lambda < 0.11$ and $a/\lambda < 0.4$. Although the total number of the polarization conversion bands (within the same frequency range) is usually larger for the mesh-free structures, those with the mesh often allow a better approaching to the case of perfect polarization conversion.

The resonance frequencies corresponding to the first maxima of $|T^f_{xy}|$ in **Figure 3(c, e, g, i)** are approximated by

$$f = f_{(0)}\varepsilon^{-0.36}, \tag{8}$$

where $f_{(0)}$ stands for the resonance frequency at ε = 1. If a wider range of ε variation is considered (i.e., $\varepsilon_{\max} > 11.4$), 0.36 in Eq. (8) must be replaced with a larger value, e.g., with 0.39 [1]. For a more accurate approximation, subranges of larger ε and smaller ε should be considered separately. In turn, for the both maxima of $|T^f_{yx}|$ from the first pair in **Figure 3(b, d, f, h)**, the following approximation can be used:

$$f = f_{(0)}\varepsilon^{-0.33}. \tag{9}$$

Thus, comparing with the classical scaling rule of $\varepsilon^{-1/2}$, one obtains similar rules for the basic configuration, so that the effect of variations in ε can be quantified. Surprisingly, the appropriate exponent values differ from the classical rule not strongly, although a large part of the resonance field energy may correspond to the exterior of subwavelength resonators. Moreover, not only locations of the maxima but also separation between them, Δf, can be predicted for different values of ε. In terms of the Lagrange model, a decrease in Δf at larger ε indicates a weaker coupling that might be connected with a larger electrical thickness of the dielectric substrate and a larger phase difference at the opposite sides of a dielectric layer.

A simultaneous widening of two polarization conversion bands can be achieved in the basic configuration just by modification of the metallic mesh parameters. **Figure 4** presents an example, in which the mesh has a larger period than that shown in **Figure 3**. In fact, this structure differs from that in **Figure 3(i)** only in the values of p and h. One can see that the second band of $|T^f_{xy}| = |T^b_{yx}| \approx 1$ in the vicinity of $f = 6.4$ GHz is similar to such bands shown in **Figure 3(g, i)**. However, the first band (at $f = 2.8$ GHz) has now two neighboring maxima with a very weak dip between them, so that our guess regarding a possible nature of the single maxima observed in the structures with the mesh in **Figure 3** may be correct. Note that the values of $|T^f_{yx}| = |T^b_{xy}|$ can also be quite large within the bands of $|T^f_{xy}| = |T^b_{yx}| \approx 1$, as shown in **Figure 4(b)** at f = 6.5 GHz. In this case, nearly perfect two-way polarization conversion is obtained, i.e., it occurs for both incident linear polarizations. Thus, both one-way and two-way polarization conversion bands can appear in one structure. Besides, it is interesting to compare locations of the maxima in **Figures 3(i)** and **4(b)**, while p is varied but the total volume occupied by a metal is fixed. The first band is shifted from $f = 2.66$ GHz to the vicinity of $f = 2.8$ GHz (two close maxima at 2.78 and 2.84 GHz, with a weak dip between them). The second band is shifted from the vicinity of f = 5.75 GHz to the vicinity f = 6.4 GHz. Hence, the introduced modification of the mesh geometry leads to the enhancement of the capacitive effect for the both broadbands.

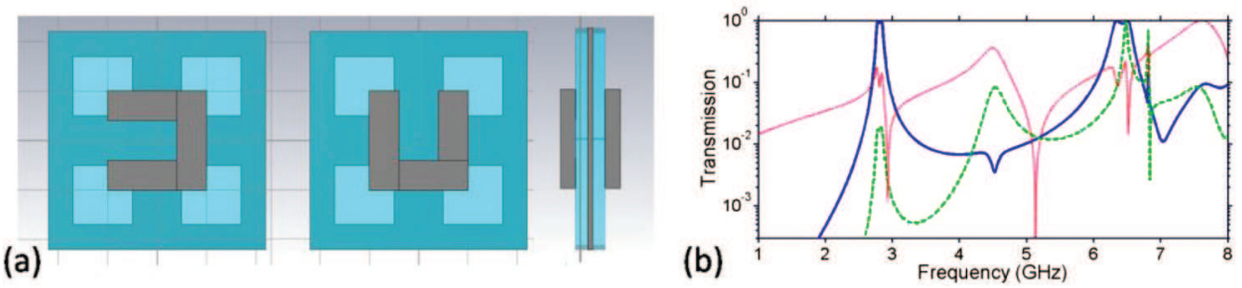

Figure 4. (a) Front, back, and side view of a unit cell, and (b) transmission for the basic configuration with a modified metallic mesh, $p = 11$ mm and $h = 6$ mm: solid blue line – $|T^f_{xy}| = |T^b_{yx}|$, dashed green line – $|T^f_{yx}| = |T^b_{xy}|$, and dotted red line – $|T^f_{xx}| = |T^b_{xx}| = |T^f_{yy}| = |T^b_{yy}|$; $\varepsilon = 11.4$.

3.2. Thin and thick configurations

Next, we consider the structures with a smaller and a larger distance between the coupled metasurfaces. Results for the structures with $L_1 = L_2 = 0.25$mm, $s_3 = 0.5$mm, and the same remaining parameters as for the basic configuration are presented in **Figure 5**. Now, we have $S = 2$mm, so that we refer to it as *thin configuration*. First, one should notice that separation of the resonances is here stronger pronounced than for the basic configuration. Generally, it may occur because each metasurface strongly affects the resonance field of the other in the thin configuration, leading to a stronger coupling. For example, the difference in location of the maxima observed in **Figure 5(b)** for the mesh-free structure with $\varepsilon = 2.1$ is larger than 2 GHz. In this case, the maximal values for two cross-polarized components are close to each other, while the copolarized components are not suppressed at the resonances.

Introducing a metallic mesh between the metasurfaces results in that the distance between the maxima dramatically decreases. Indeed, the center frequency $f_0 = (f_u + f_l)/2$, where f_u and f_l are the upper and the lower frequencies in a pair of the coupled (neighboring) resonances, is

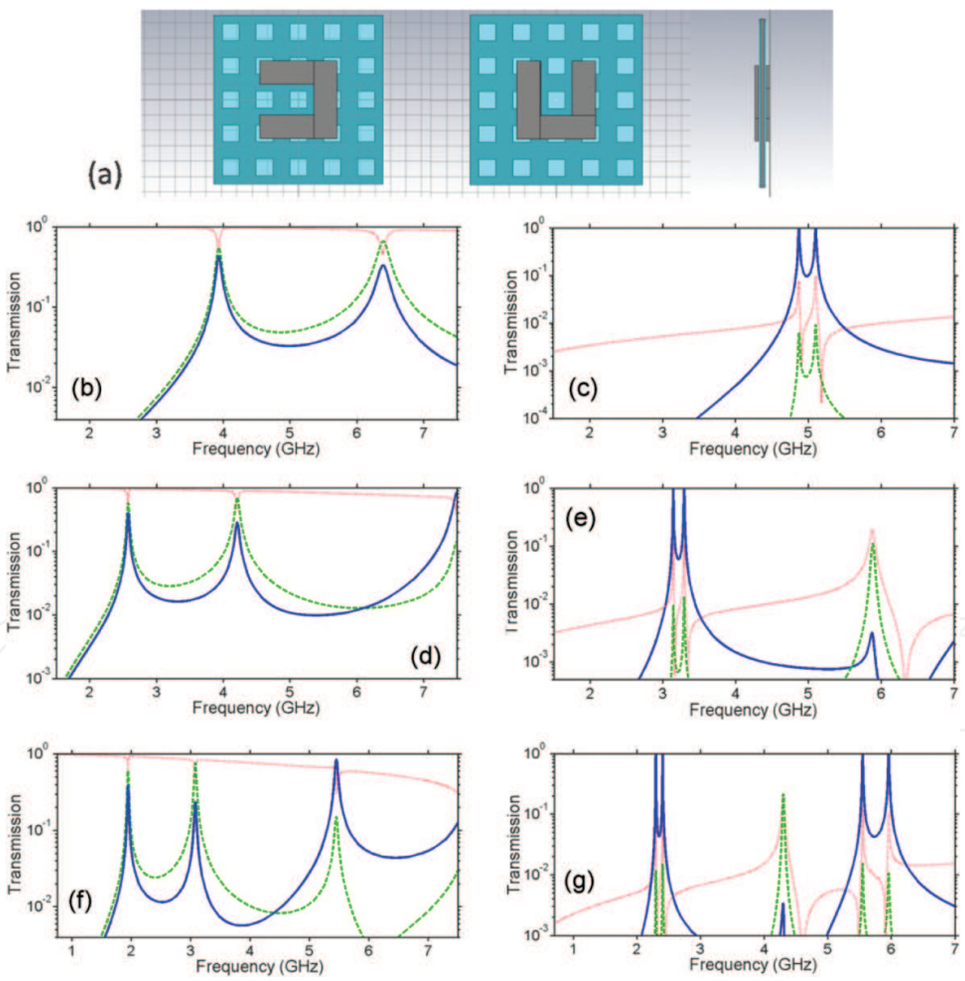

Figure 5. (a) Front, back, and side view of a unit cell, and transmission for the thin configuration (b, d, f) without and (c, e, g) with metallic mesh; (b, c) $\varepsilon = 2.1$, (d, e) $\varepsilon = 5.8$, (f, g) $\varepsilon = 11.4$; solid blue line – $|T^f_{xy}| = |T^b_{yx}|$, dashed green line – $|T^f_{yx}| = |T^b_{xy}|$, and dotted red line – $|T^f_{xx}| = |T^b_{xx}| = |T^f_{yy}| = |T^b_{yy}|$.

equal to 5.16 and 4.99 GHz in **Figure 5(b)** and **Figure 5(c)**, respectively, i.e., the shift is not very strong. At the same time, $\Delta f = f_u - f_l$ is 2.45 and 0.23 GHz, i.e., the difference between two structures in terms of resonance separation is very strong. For the mesh-free structures in **Figure 5(b, d, f)**, these features are in agreement with the predictions based on the Lagrange model (f_u and f_l correspond to ω_+ and ω_-): stronger coupling appears at smaller distances between the SRRs [41, 42]. On the other hand, assuming that the spectral separation of the neighboring maxima is connected with the strength of resonance coupling for a wider class of the structures, one may expect that in the mesh-containing structures in **Figure 5(c, e, g)**, the coupling is substantially weaker because of the effect exerted by the mesh. This feature probably originates from the fact that the mesh prevents direct coupling of nonevanescent waves at two sides of the entire structure. Similarly to **Figure 3**, nearly perfect polarization conversion and related diodelike transmission are obtained for the mesh-containing structures in **Figure 5**. Moreover, on the contrary to **Figure 3**, $|T^f_{xy}| > 0.99$ is achieved in a very wide range of variation of ε, while other components of the T-matrix are weak.

An increase of ε only leads to the resonance redshift, so that a larger number of narrow bands of polarization conversion might appear at the subwavelength range. Four nearly perfect maxima of $|T^f_{xy}|$ are observed in **Figure 5(g)** at ε = 11.4. Accordingly, Δf is decreased for each pair of the coupled resonances. For instance, for the first pair of resonances, we obtain $\Delta f = f_u - f_l$ = 0.15GHz and 1.64GHz in the structures with and without mesh at ε = 5.8, see **Figure 5(d, e)** and Δf = 0.11GHz and 1.14GHz for similar structures at ε = 11.4, see **Figure 5(f, g)**. Hence, a strong effect of the metallic mesh on coupling and location of high-Q resonances is typical at small distances between metasurfaces. Whereas obtaining nearly perfect polarization conversion does not need a special choice of substrate materials in the mesh-containing structures with small distance between metasurfaces, obtaining a near-unity cross-polarized component in similar mesh-free structures is a more challenging task.

The resonance frequencies corresponding to the first maxima of $|T^f_{yx}|$ in **Figure 5(b, d, f)** can be approximated by Eq. (9) but with the exponent of -0.375 instead of -0.33. For the first and second maxima of $|T^f_{xy}|$ (in the first pair) in **Figure 5(c, e, g)**, it is recommended to use Eq. (8) with -0.42 instead of -0.36. Note that the difference in the exponent required in the case of mesh free and mesh-containing structures is increased as compared to the basic configuration. Qualitatively, a better approaching to the value of -1/2 that is observed for the thin structures with the mesh means that the resonance fields are strongly localized and, thus, they may correspond to larger values of Q. Indeed, one can see that the resonances are sharper in **Figure 5** than in **Figure 3**. One should keep in mind that high-Q resonances can be more sensitive to the Ohmic losses, leading to undesired absorption enhancement and suppression of the transmission maxima [16].

Now, we consider *thick configuration*, which differs from the basic one in that $L_1 = L_2$ = 2.5mm and, thus, S = 8.5mm, see **Figure 6**. Compared to **Figures 3** and **5**, the mesh-containing structures seem now less appropriate for high-efficiency polarization conversion. Indeed, conversion is typically far from the perfect one, whereas reflections are quite strong. For

http://dx.doi.org/10.5772/65950

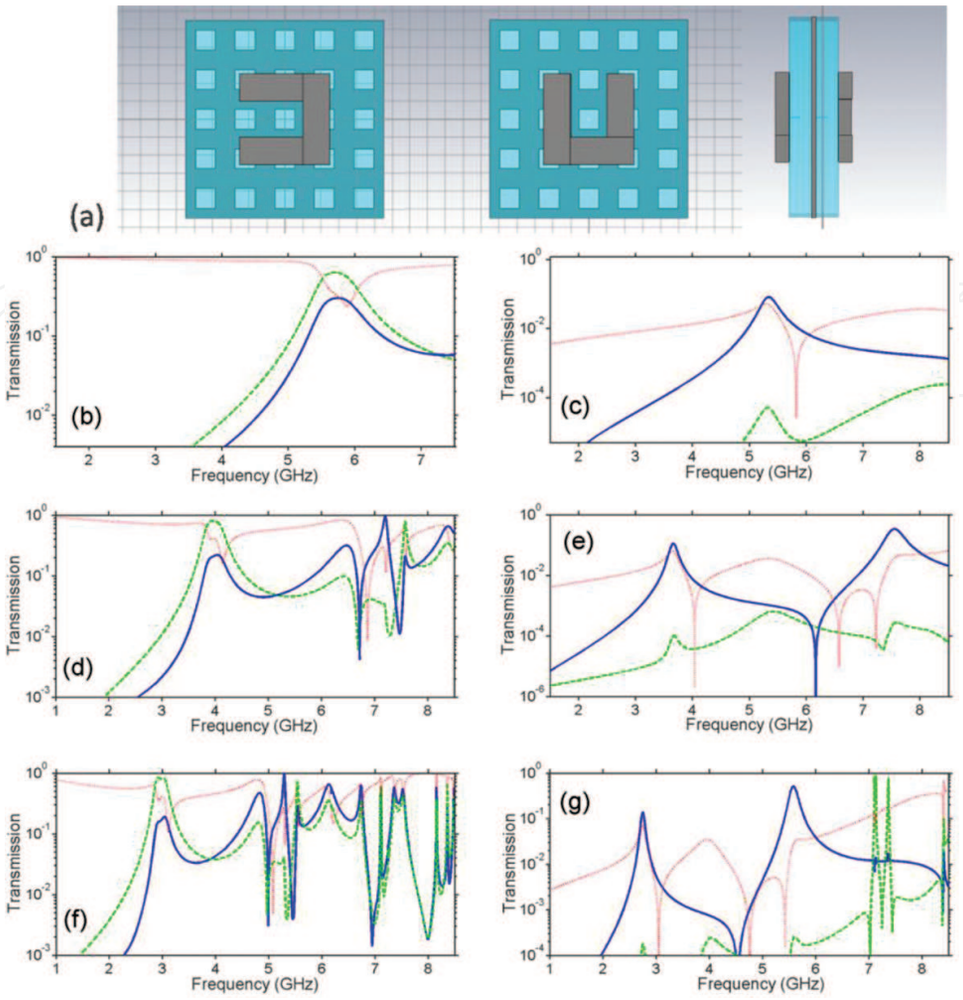

Figure 6. (a) Front, back, and side view of a unit cell, and transmission for the thick configuration (b, d, f) without and (c, e, g) with metallic mesh; (b, c) ε = 2.1, (d, e) ε = 5.8, (f, g) ε = 11.4; solid blue line – $|T^f_{xy}| = |T^b_{yx}|$, dashed green line – $|T^f_{yx}| = |T^b_{xy}|$, and dotted red line – $|T^f_{xx}| = |T^b_{xx}| = |T^f_{yy}| = |T^b_{yy}|$.

instance, in **Figure 6(e)** we obtain $|T^f_{xy}|\approx 0.11$ and $|T^f_{xy}|\approx 0.33$ at f = 3.65 and f = 7.55 GHz. In **Figure 6(g)**, $|T^f_{xy}|\approx 0.14$ and $|T^f_{xy}|\approx 0.51$ at f = 2.74 and f = 5.57 GHz, respectively, and $|T^f_{yx}| > 0.96$ at the two narrow maxima near f = 7.12 GHz (separation is about 25 MHz). At the same time, the mesh-free structures enable high-efficiency conversion and rather wide bands already at ε = 5.8 and, thus, can be more useful. For example, $|T^f_{yx}|\approx 0.79$ and $|T^f_{xy}| > 0.96$ at f = 3.9 and f = 7.2 GHz in **Figure 6(d)**. To compare, in **Figure 6(f)**, $|T^f_{yx}| > 0.8$ at f = 2.89 GHz and $|T^f_{xy}| > 0.95$ at f = 5.29 GHz, for ε = 11.4.

As follows from the comparison of **Figure 6(b, d, f)** with **Figure 6(c, e, g)**, the case of a large distance between metasurfaces in combination with the evanescent-wave regime of the metallic mesh is less appropriate for the practical use. At the same time, polarization conversion can be obtained in such structures for two different polarization states of the incident wave, see **Figure 6(g)**. Hence, this is not a unique property of the mesh-free structures, compare to

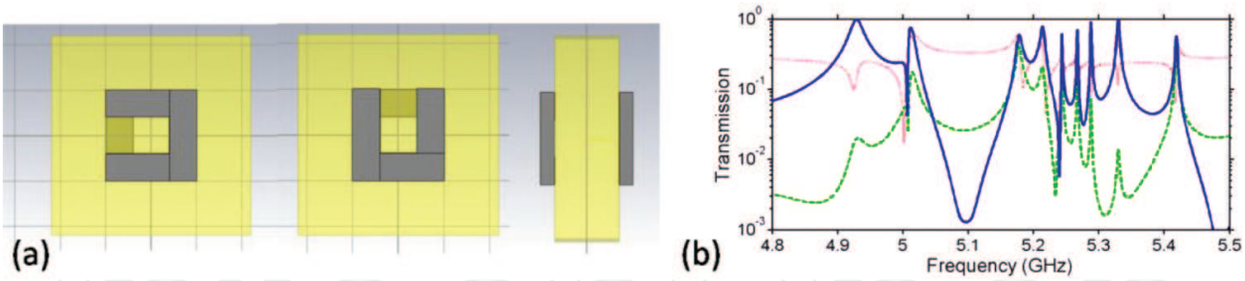

Figure 7. (a) Front, back, and side view of a unit cell, and transmission for the thick configuration with $L = d + L_1 + L_2 = 11mm$ and $S = 14mm$, and (b) transmission in the case without metallic mesh, ε = 35.4; solid blue line – $|T^f_{xy}| = |T^b_{yx}|$, dashed green line – $|T^f_{yx}| = |T^b_{xy}|$, and dotted red line – $|T^f_{xx}| = |T^b_{xx}| = |T^f_{yy}| = |T^b_{yy}|$.

Figures 3 and **5**. Regardless of this, the combination of variations in ε with those in L_1 and L_2 gives a big freedom for design. Also in this case, a scaling rule can be introduced, in the analogy with the rule of $\varepsilon^{-1/2}$ and Eqs. (8) and (9). For instance, for the first maximum of $|T^f_{xy}|$ in **Figure 6(c, e, g)** one can use Eq. (8), in which 0.36 is replaced with 0.23. This approximation is very rough, and the use of other functions than the exponential one may give a much better result in this case. However, it demonstrates the main trend quite correctly: the thicker the dielectric layers, the stronger the deviation from the rule of $\varepsilon^{-1/2}$.

Let us check whether an increase of L up to the values, at which classical Fabry-Perot resonances may appear in the dielectric layers, can improve the performance in terms of polarization conversion and asymmetric transmission. As an example, **Figure 7** presents the results for the structure, which is distinguished from those in **Figures 3(b, d, f, h)** and **6(b, d, f)** only in the values of ε and L. Transmission is shown for a high-frequency range, in which the multiple bands of one-way polarization conversion are located. For instance, the maxima of $|T^f_{xy}|\approx 0.98$ and $|T^f_{xy}|\approx 0.975$ are observed at f = 4.93 and f = 5.32 GHz, where $S/\lambda = 0.164$ and $\varepsilon^{1/2}L/\lambda = 0.68$, and $S/\lambda = 0.178$ and $\varepsilon^{1/2}L/\lambda = 0.74$, respectively. Hence, Fabry-Perot type interferences may, in principle, contribute to the resulting polarization conversion mechanism, although analytical description of this regime would require taking into account the effective contribution of SRRs. One can see that the maxima of $|T^f_{xy}|$, at which diodelike asymmetric transmission is well pronounced, are connected with the different resonances whose Q-factors may be strongly distinguished from each other. It follows from the obtained results in **Figure 7** that the mesh-free structures with thick dielectric layers may enable a nearly perfect multiband polarization conversion.

3.3. Role of array period

In addition, the effects exerted by variations of the substrate parameters on transmission and polarization conversion are sensitive to the array period, a. Changing the period, we change the distance between the neighboring subwavelength resonators in each metasurface. The same is related to the resonators belonging to the adjacent unit cells and different metasurfaces. Thus, it may be expected that such changes affect coupling and, hence, locations and manifestations of polarization conversion resonances. In **Figure 8**, the results are

http://dx.doi.org/10.5772/65950

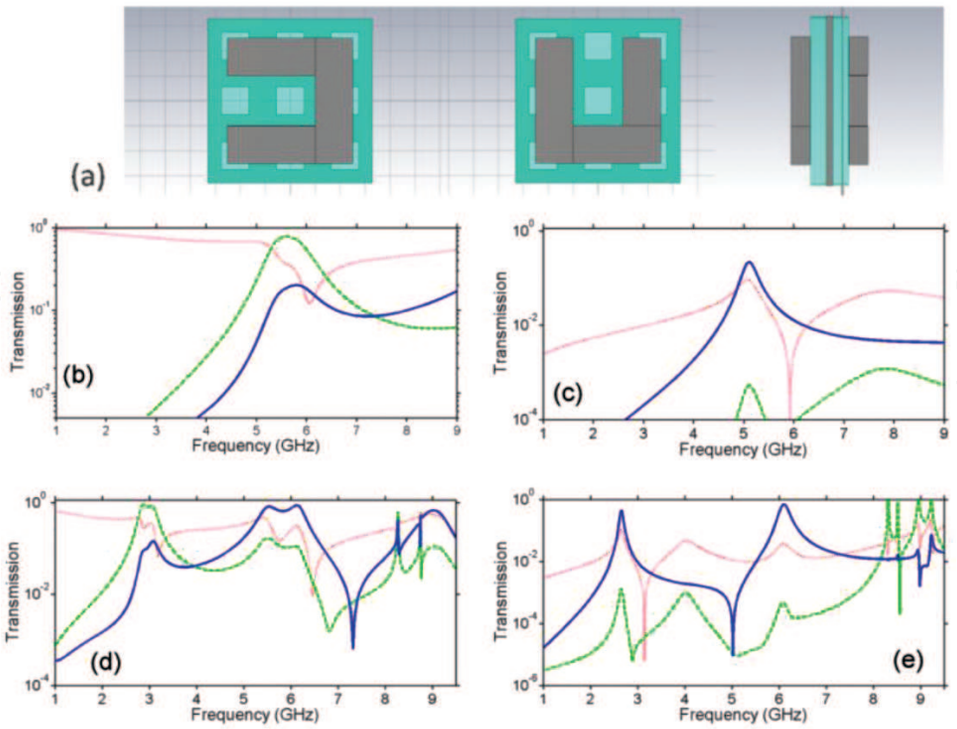

Figure 8. (a) Front, back, and side view of a unit cell, and transmission at a small array period, $a = 3p$, in cases (b, d) without and (c, e) with metallic mesh; (b, c) $\varepsilon = 2.1$, (d, e) $\varepsilon = 11.4$; solid blue line – $|T^f_{xy}|$, dashed green line – $|T^f_{yx}|$, and dotted red line – $|T^f_{xx}| = |T^f_{yy}|$.

presented for four structures, which differ from the basic configuration in that now $a = 3p$, while the remaining parameters are the same. Accordingly, $a/\lambda < 0.5$ at $f < 11.3$ GHz. Surprisingly, the obtained dependences are similar to the case of thick dielectric layers in **Figure 6**. This occurs for both the mesh-free and the mesh-containing structures. Thus, the former allow one obtaining high-efficiency polarization conversion starting from smaller values of ε than the latter. At the same time, as seen in **Figure 8(d, e)**, ε=11.4 is large enough for obtaining efficient polarization conversion and asymmetric transmission in the structures both with and without a mesh.

Finally, we consider the case of a larger array period, $a = 7p$, while the remaining parameters are the same as for the basic configuration in **Figure 3**. The results are presented in **Figure 9**. Now, $a/\lambda < 0.5$ at $f < 4.87$ GHz. Thus, higher diffraction orders may propagate at normal incidence starting from 9.74 GHz. The basic features are not changed, as compared to **Figures 3** and **6**. High-efficiency polarization conversion is observed in the mesh-containing structures with $\varepsilon = 2.1$ and $\varepsilon = 11.4$, see **Figure 9(c, e)**, and in the mesh-free structures at $\varepsilon = 11.4$, see **Figure 9(d)**. In particular, the first and second maxima with $|T^f_{yx}| > 0.8$ can be achieved in the mesh-free structure in **Figure 9(d)**. In the mesh-containing structures, $|T^f_{xy}| > 0.96$ and $|T^f_{xy}| > 0.99$ is obtained for the first maximum in **Figure 9(c)** and **Figure 9(e)**, respectively. Hence, high-efficiency transmission may occur even when the distance between the neighboring SRRs of the same metasurface is rather large. Thus, the energy can be *harvested* from a large

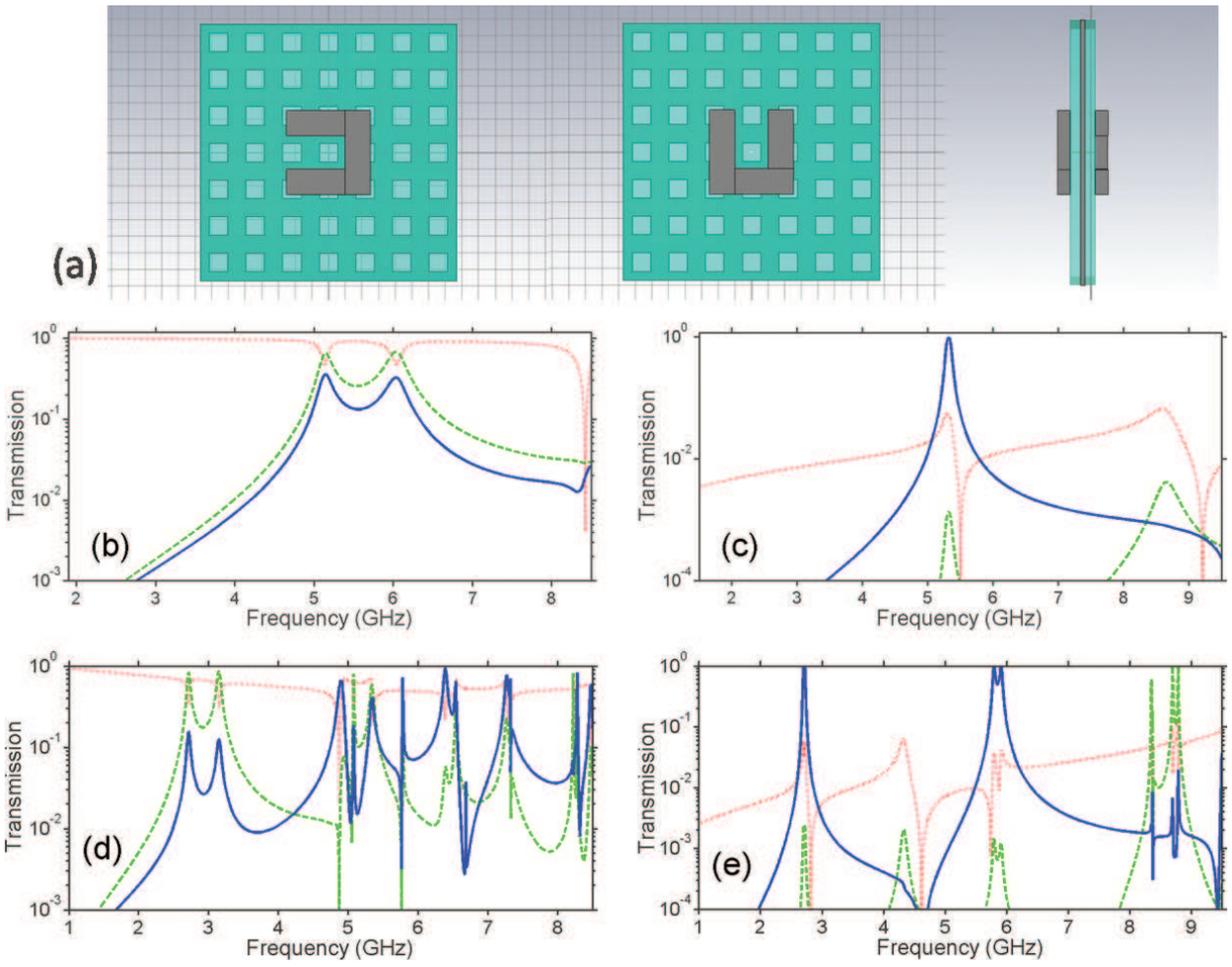

Figure 9. (a) Front, back, and side view of a unit cell, and transmission at a large array period, $a = 7p$, in cases (b, d) without and (c, e) with the metallic mesh; (b, c) $\varepsilon = 2.1$, (d, e) $\varepsilon = 11.4$; solid blue line – $|T^f_{xy}|$, dashed green line – $|T^f_{yx}|$, and dotted red line – $|T^f_{xx}| = |T^f_{yy}|$.

area and then converted into the orthogonal polarization. In other words, the coupled metasurfaces work like an *array of energy concentrators*. It is interesting that the harvesting occurs in the structures with and without a mesh. A detailed study is needed to clarify possible connection of this regime with (spoof) surface plasmons.

The effect of an array period on transmission is illustrated by the data shown in **Table 1**. One can see that spectral locations of the polarization conversion bands/maxima are rather weakly affected by the period. This indicates the dominant role of subwavelength resonances of the complex unit cells and coupling of metasurfaces owing to the resonators located at the front of each other. The array period strongly affects manifestations of the resonances, e.g., due to the difference in the value of Q. The presence of the mesh may lead to strong polarization conversion at the other incident polarization than in the corresponding mesh-free structures for all three values of the period. Nevertheless, the dominant effect of subwavelength resonances of the unit cells on the location of the polarization conversion bands/maxima remains in all of the cases studied.

Small array period, $a = 3p$	**Basic array period, $a = 5p$**	**Large array period, $a = 7p$**
	Structure without mesh, $\varepsilon = 2.1$	
Band of $\lvert T^f_{yx}\rvert$ around 5.58 GHz	Two maxima of $\lvert T^f_{yx}\rvert$ at 5.27 and 6.09 GHz	Two maxima of $\lvert T^f_{yx}\rvert$ at 5.15 and 6.04 GHz
	Structure with mesh, $\varepsilon = 2.1$	
Maximum of $\lvert T^f_{xy}\rvert$ at 5.1 GHz	Maximum of $\lvert T^f_{xy}\rvert$ at 5.31 GHz	Maximum of $\lvert T^f_{xy}\rvert$ at 5.32 GHz
	Structure without mesh, $\varepsilon = 11.4$	
Band of $\lvert T^f_{yx}\rvert$ around $f = 2.95$ GHz	Two maxima of $\lvert T^f_{yx}\rvert$ at 2.76 and 3.17 GHz	Two maxima of $\lvert T^f_{yx}\rvert$ at 2.71 and 3.15 GHz
	Structure with mesh, $\varepsilon = 11.4$	
Two maxima of $\lvert T^f_{xy}\rvert$ at 2.66 and 6.1 GHz	Maximum at 2.66 GHz and twin maximum at 5.72/5.82 GHz for $\lvert T^f_{xy}\rvert$	Twin maximum at 2.701/2.717 GHz and twin maximum at 5.8/5.91 GHz for $\lvert T^f_{xy}\rvert$

Table 1. Comparison of the bands/transmission maxima at which polarization conversion takes place, for $a = 3p$, $a = 5p$, and $a = 7p$; $p = 4.4$ mm.

4. Concluding remarks

To summarize, dielectric substrate parameters can strongly affect polarization conversion and asymmetric transmission regimes achievable in low-profile structures comprising two coupled metasurfaces that represent arrays of subwavelength resonant elements. The comparison has been carried out for the structures with and without metallic mesh and, thus, with and without tunneling. It has been demonstrated that sometimes the former and sometimes the latter can be preferable for the practical use. Perfect polarization conversion usually means that asymmetry in transmission is also perfect, and vice versa. This remains true at least if higher diffraction orders in the hosting air space are evanescent. The obtained results illustrate the main similarities and differences of the cases of a low-ε and high-ε substrate, a thin and thick dielectric layer, and a large and small array period. The role of a dielectric substrate that is directly adjusted to the subwavelength resonators is to modify the resonances that are located in the subwavelength range and shift more resonances to this range. Thus, it is far beyond of being just a mechanical support for metallic elements. In the case of small thickness of dielectric layers, the ability of preserving the secondary electromagnetic characteristics related to transmission and polarization is very general. This means that the required phase-matching conditions that may result in a nearly perfect transmission in the structures with a mesh can be satisfied in a wide range of ε-variation. This enables a scaling rule, which differs from the classical rule of $\varepsilon^{-1/2}$, while the polarization and transmission characteristics are preserved. The same remains true for the impedance-matching conditions in the structures without a mesh. Generally speaking, tunneling as a part of the resulting conversion mechanism is not necessary but desirable in many cases. For the fabrication reasons, structures with rather thick dielectric layers might be preferable. Moreover, thick layers help to obtain wider bands of

polarization conversion, which are however not perfect. Unfortunately, conditions of nearly perfect polarization conversion are not satisfied for these structures in a wide ε-range, while thickness is fixed. Hence, more accurate adjustment of geometrical parameters is needed for a given material. In spite of this, variations in ε remain an efficient tool for manipulation by subwavelength resonances and related polarization conversion. The presented results give one useful guidelines, which are hopefully sufficient at least for initial-stage design. It is noteworthy that the resulting structures are electrically thin, e.g., $S/\lambda < 1/10$ and even $S/\lambda < 1/30$ for the selected operation regimes, when a substrate with $\varepsilon > 5$ is utilized. Although the zero-loss approximation has been used here, the basic effects are expected to remain when the actual Ohmic losses are taken into account, at least if Q-factor is not very high (i.e., resonances in zero-loss approximation are not very sharp). In particular, substrate parameters should exert a strong effect on the resulting performance at microwave, terahertz, and, probably, infrared frequencies. Finally, it should be noted that polarization conversion regimes that involve circular polarization can also be efficiently controlled by variations of the substrate parameters, while the individual metasurfaces are kept without change.

Acknowledgements

A.E.S. thanks the National Science Centre of Poland for financial assistance under the project MetaSel DEC-2015/17/B/ST3/00118, and TUBITAK for partial support in the framework of the Visiting Researcher Program. A part of this work is supported by the projects DPT-HAMIT, ESF-EPIGRAT, and NATO-SET-181, and by TUBITAK under the project nos. 107A004, 109A015, and 109E301. E.O. acknowledges partial support from the Turkish Academy of Sciences.

Author details

Andriy E. Serebryannikov[1]*, Mehmet Mutlu[2] and Ekmel Ozbay[2]

*Address all correspondence to: andser@amu.edu.pl

1 Faculty of Physics, Adam Mickiewicz University, Poznań, Poland

2 Nanotechnology Research Center—NANOTAM, Bilkent University, Ankara, Turkey

References

[1] Serebryannikov AE, Mutlu M, Ozbay E. Dielectric inspired scaling of polarization conversion subwavelength resonances in open ultrathin chiral structures. Appl. Phys. Lett. 2015;**107**:221907. DOI: 10.1063/1.4936603

[2] Gan X, Shiue RJ, Gao Y, Assefa S, Hone J, Englund D. Controlled light–matter interaction in graphene electrooptic devices using nanophotonic cavities and waveguides. IEEE Trans. Select. Top. Quant. Electron. 2014;**20**:6000311. DOI: 10.1109/JSTQE.2013.2273412

[3] Song K, Liu Y, Fu Q, Zhao X, Luo C, Zhu W. 90° polarization rotator with rotation angle independent of substrate permittivity and incident angles using a composite chiral metamaterial. Opt. Express. 2013;**21**:7439–7446. DOI: 10.1364/OE.21.007439

[4] Song K, Zhao X, Li Y, Fu Q, Luo C. A frequency-tunable 90°- polarization rotation device using composite chiral metamaterials. Appl. Phys. Lett. 2013;**103**:101908. DOI: 10.1063/1.4820810

[5] Yao Y, Kats MA, Shankar P, Song Y, Kong J, Loncar M, Capasso F. Wide wavelength tuning of optical antennas on graphene with nanosecond response time. Nano Lett. 2014;**14**:214–219. DOI: 10.1021/nl403751p

[6] Pendry JB. Negative refraction makes a perfect lens. Phys. Rev. Lett. 2000;**85**:3966–3969. DOI: 10.1103/PhysRevLett.85.3966

[7] Pendry JB. A chiral route to negative refraction. Science. 2004;**306**:1353–1355. DOI: 10.1126/science.1104467

[8] Kriegler CE, Rill MS, Linden S, Wegener M. Bianisotropic photonic metamaterials. IEEE Trans. Select. Top. Quant. Electron. 2010;**16**:367–375. DOI: 10.1109/JSTQE.2009.2020809

[9] Liu N, Liu H, Zhu S, Giessen H. Stereometamaterials. Nat. Photon. 2009;**3**:157–162. DOI: 10.1038/nphoton.2009.4

[10] Mutlu M, Akosman AE, Ozbay E. Broadband circular polarizer based on high-contrast gratings. Opt. Lett. 2012;**37**:2094–2096. DOI: 10.1364/OL.37.002094

[11] Torres V, Sanchez N, Etayo D, Ortuno D, Navarro-Cia M, et al. Compact dual-band terahertz quarter-wave plate metasurface. IEEE Photon. Technol. Lett. 2014;**26**:1679–1682. DOI: 10.1109/LPT.2014.2330860

[12] Li Z, Liu W, Cheng H, Chen S, Tian J. Realizing broadband and invertible linear-to-circular polarization converter with ultrathin single-layer metasurface. Sci. Rep. 2015;**5**:18106. DOI: 10.1038/srep18106

[13] Cheng H, Chen S, Yu P, Li J, Deng L, Tian J. Mid-infrared tunable optical polarization converter composed of asymmetric graphene nanocrosses. Opt. Lett. 2013;**38**:1567–1569. DOI: 10.1364/OL.38.001567

[14] Pfeiffer C, Zhang C, Ray V, Guo LJ, Grbic A. High-performance bianisotropic metasurfaces: asymmetric transmission of light. Phys. Rev. Lett. 2014;**113**:023902. DOI: 10.1103/PhysRevLett.113.023902

[15] Zhao Y, Belkin MA, Alu A. Twisted optical metamaterials for planarized ultrathin broadband circular polarizers. Nat. Commun. 2012;**3**:870. DOI: 10.1038/ncomms1877

[16] Fedotov VA, Mladyonov PL, Prosvirnin SL, Rogacheva AV, et al. Asymmetric propagation of electromagnetic waves through a planar chiral structure. Phys. Rev. Lett. 2006;**97**:167401. DOI: 10.1103/PhysRevLett.97.167401

[17] Plum E, Fedotov VA, Zheludev NI. Planar metamaterial with transmission and reflection that depend on the direction of incidence. Appl. Phys. Lett. 2009;**94**:131901. DOI: 10.1063/1.3107264

[18] Singh R, Plum E, Menzel C, Rockstuhl C, Azad AK, Cheville RA, Lederer F, Zhang W, Zheludev NI. Terahertz metamaterial with asymmetric transmission. Phys. Rev. B. 2009;**80**:153104. DOI: 10.1103/PhysRevB.80.153104

[19] Mutlu M, Akosman AE, Serebryannikov AE, Ozbay E. Asymmetric chiral metamaterial circular polarizer based on four U-shaped split ring resonators. Opt. Lett. 2011;**36**:1653–1655. DOI: 10.1364/OL.36.001653

[20] Ma X, Huang C, Pu M, Hu C, Feng Q, Luo X. Multi-band circular polarizer using planar spiral metamaterial structure. Opt. Express. 2012;**20**:16050–16058. DOI: 10.1364/OE.20.016050

[21] Pan C, Ren M, Li Q, Fan S, Xu J. Broadband asymmetric transmission of optical waves from spiral plasmonic metamaterials. Appl. Phys. Lett. 2014;**104**:121112. DOI: 10.1063/1.4869297

[22] Menzel C, Helgert C, Rockstuhl C, Kley EB, Tuennermann A, et al. Asymmetric transmission of linearly polarized light at optical metamaterials. Phys. Rev. Lett. 2010;**104**:253902. DOI: 10.1103/PhysRevLett.104.253902

[23] Mutlu M, Akosman AE, Serebryannikov AE, Ozbay E. Diodelike asymmetric transmission of linearly polarized waves using magnetoelectric coupling and electromagnetic wave tunneling. Phys. Rev. Lett. 2012:**108**,213905. DOI: 10.1103/PhysRevLett.108.213905

[24] Serebryannikov AE. One-way diffraction effects in photonic crystal gratings made of isotropic materials. Phys. Rev. B. 2009;**80**:155117. DOI: 10.1103/PhysRevB.80.155117

[25] Li XF, Ni X, Feng LA, Lu MH, He C, Chen YF. Tunable unidirectional sound propagation through a sonic-crystal-based acoustic diode. Phys. Rev. Lett. 2011;**106**:084301. DOI: 10.1103/PhysRevLett.106.084301

[26] Serebryannikov AE, Ozbay E, Nojima S. Asymmetric transmission of terahertz waves using polar dielectrics. Opt. Express. 2014;**22**:3075–3088. DOI: 10.1364/OE.22.003075

[27] Rodriguez-Ulibarri P, Beruete M, Navarro-Cia M, Serebryannikov AE. Wideband unidirectional transmission with tunable sign-switchable refraction and deflection in non-symmetric structures. Phys. Rev. B. 2013;**88**:165137. DOI: 10.1103/PhysRevB.88.165137

[28] Feng F, Ayache M, Huang J, Xu YL, Lu MH, Chen YF, et al. Nonreciprocal light propagation in a silicon photonic circuit. Science. 2011;**333**:729–733. DOI: 10.1126/science.1206038

[29] Mutlu M, Cakmakyapan S, Serebryannikov AE, Ozbay E. One-way reciprocal spoof surface plasmons and relevant reversible diodelike beaming. Phys. Rev. B. 2013;**87**: 205123. DOI: 10.1103/PhysRevB.87.205123

[30] Serebryannikov AE, Cakmak AO, Ozbay E. Multichannel optical diode with unidirectional diffraction relevant total transmission. Opt. Express. 2012;**20**:14980–14990. DOI: 10.1364/OE.20.014980

[31] Markovich DL, Andriyieuski A, Zalkovskij M, et al. Metamaterial polarization convertor analysis: limits of performance. Appl. Phys. B. 2013;**112**:143–152. DOI: 10.1007/s00340-013-5383-8

[32] Serebryannikov AE, Beruete M, Mutlu M, Ozbay E. Multiband one-way polarization conversion in complementary split-ring resonator based structures by combining chirality and tunneling. Opt. Express. 2015;**23**:13517–13529. DOI: 10.1364/OE.23.013517

[33] Li Z, Chen S, Tang C, Liu W, Cheng H, et al. Broadband diodelike asymmetric transmission of linearly polarized light in ultrathin hybrid metamaterial. Appl. Phys. Lett. 2014;**105**:201103. DOI: 10.1063/1.4902162

[34] Shi J, Liu X, Yu S, Vu T, Zhu Z, Ma HF, Cui TJ. Dual-band asymmetric transmission of linear polarization in bilayered metamaterial. Appl. Phys. Lett. 2013;**102**:191905. DOI: 10.1063/1.4773516

[35] Shi JH, Ma HF, Guan CY, Wang ZP, Cui TJ. Broadband chirality and asymmetric transmission in ultrathin 90˚-twisted Babinet-inverted metasurfaces. Phys. Rev. B. 2014;**89**:165128. DOI: 10.1103/PhysRevB.89.165128

[36] Xu HX, Wang GM, Qi MQ, Cai T, Cui TJ. Compact dual-band circular polarizer using twisted Hilbert-shaped planar metamaterials. Opt. Express. 2013;**21**:24912–24921. DOI: 10.1364/OE.21.024912

[37] Zhou L, Wen W, Chan CT, Cheng P. Electromagnetic-wave tunneling through negative-permittivity media with high magnetic fields. Phys. Rev. Lett. 2005;**94**:243905. DOI: 10.1103/PhysRevLett.94.243905

[38] Hou B, Wen H, Leng Y, Wen W. Electromagnetic wave transmission through subwavelength metallic meshes sandwiched between split rings. Appl. Phys. Lett. 2005;**87**:201114. DOI: 10.1063/1.2133915

[39] Sun W, He Q, Hao J, Zhou L. A transparent metamaterial to manipulate electromagnetic wave polarizations. Opt. Lett. 2011;**36**:927–929. DOI: 10.1364/OL.36.000927

[40] Semouchkina E. Development of miniature microwave components by using high contrast dielectrics. In: Minin I, editor. Microwave and Millimeter Wave Technologies from Photonic Bandgap Devices to Antenna and Applications. Intech; Rijeka. 2010. pp. 231–256. DOI: 10.5772/9062

[41] Li TQ, Liu H, Li T, Wang SM, Wang FM, Wu RX, Chen P, et al. Magnetic resonance hybridization and optical activity of microwaves in a chiral metamaterial. Appl. Phys. Lett. 2008;**92**:131111. DOI: 10.1063/1.2905285

[42] Liu N, Liu H, Zhu S, Liu H, Genov DA, Wu DM, et al. Magnetic plasmon hybridization and optical activity at optical frequencies in metallic nanostructures. Phys. Rev. B. 2007;**76**:073101. DOI: 10.1103/PhysRevB.76.073101

[43] Liu H, Cao JX, Zhu SN, Liu N, Ameling R, Giessen H. Lagrange model for the optical properties of stereometamaterials. Phys. Rev. B. 2010;**81**:241403. DOI: 10.1103/PhysRevB.81.241403